J. Fluid Mech. (1984), *vol.* 144, *pp.* 217–229
Printed in Great Britain

Secondary current and river-meander formation

By PETER K. KITANIDIS AND JOHN F. KENNEDY
Institute of Hydraulic Research, The University of Iowa, Iowa City, Iowa 52242

(Received 6 September 1983)

A small-perturbation stability analysis is developed for investigation of the role of the secondary current accompanying channel curvature in the initiation and early development of meanders of alluvial and ice- or rock-incised streams. A small sinusoidal perturbation in the channel alignment of an initially straight prismatic channel is introduced. The velocity of the secondary flow is calculated for uniform quasi-steady flow conditions by application of the equation of the conservation of moment of momentum. The formulation is then closed by introducing the assumption that the differential, between the outer and inner banks, rate of boundary erosion, dissolution or melting (for incised channels) or sediment discharge (for alluvial channels) is proportional to the strength of the secondary flow. This formulation leads to a linear differential equation which is solved for its orthogonal components, which give the rates of meander growth and downstream migration. It is shown that the amplitude of the meanders tends to increase and that the meanders migrate downstream. The dominant wavelength and the corresponding phase shift between channel meandering and the velocity of the spiral motion are calculated as those corresponding to the fastest growth rate. The results are found to be in good agreement with data reported by others.

1. Introduction

Practically all streams flowing in channels formed by the flows themselves exhibit an engaging feature: their channels are seldom straight along reaches of more than a few channel widths. Instead, alluvial, rock-incised and supraglacial meltwater streams are all observed to form the well-known, sinuous, migrating, successive channel curves known as meanders. Elucidation and formulation of the mechanisms responsible for stream meandering has been the subject of continuing inquiry for well over a century (Kelvin 1876). However, it is only relatively recently (notably since Leliavsky 1955; see p. 122) that the critical role of the secondary current, produced by the interaction of the curvature and the vertical gradient of the primary-flow velocity, has been fully appreciated. Moreover, there is still not general accord among investigators that the secondary current is the dominant mechanism responsible for meandering, or how it should be treated mathematically (see e.g. Ikeda, Parker & Sawai 1981; Parker, Sawai & Ikeda 1982; Falcón Ascanio & Kennedy 1983).

Zimmermann & Kennedy (1978, p. 34) describe the role of secondary currents in alluvial-channel meandering as follows:

> Near the bed, where the concentration of transported sediment is higher, the secondary current moves sediment inward across the channel and deposits some of it near the inside of the bend, while the concave bank is subjected to the erosive attack of the sediment-deficient fluid from the upper levels of the stream and the bed near the outside bank is scoured. It is this pattern of scour and deposition produced by the secondary flow that leads to the

increase in channel sinuosity and that produces the transverse bed slope that is one of the dominant characteristics of alluvial channel meanders. Accordingly, any analytical model of flow in river bends must include a mathematical description of the secondary flow and its effect on the local direction and rate of sediment transport.

Falcón Ascanio & Kennedy (1983) argue further that in strongly meandering channels (i.e. those with large-amplitude meanders), it is the greater streamwise velocity near the outer (concave) bank and the bank caving, both produced by the larger local depth there, and not the secondary current itself, that produces erosion along the outsides of channel bends.

It appears that the secondary current may also be responsible for the formation, growth and migration of meanders in incised channels in ice and rock. The spiralling secondary flow transports near-surface fluid with its greater primary-flow velocity to and along the outer banks and nearby bed, and thereby subjects these regions to intensified erosion or melting. In the case of ice channels, the secondary current along the free surface also advects heat, transferred from the air to the flowing liquid, to the outer-bank region of the channel, and further increases the melting rate there.

Reviews of the extensive literature on free-surface flow in curved or meandering channels have been presented by Callandar (1968, 1978) and Falcón Ascanio (1979). Of particular interest are the stability analyses which examine the initiation and early development of meanders. Such analyses have been presented by Hansen (1967), Callandar (1968), Engelund & Skovgaard (1973), Hayashi (1973), Parker (1975, 1976), Ikeda *et al.* (1981), Parker *et al.* (1982) and others. Most of these deal with mechanisms other than the secondary current associated with channel curvature. For example, Parker (1975) utilized potential-flow theory to study the effects on channel geometry of the primary-flow-velocity perturbations produced by standing waves.

The small-perturbation stability analysis developed here investigates the role of the secondary current in the initiation and early development of meanders in alluvial and ice- and rock-incised channels. The first step of the analysis is calculation of the streamwise distribution of the strength of the secondary current in flow in a rectangular channel with sinusoidal centreline. A closure relation then is adopted to relate the *differential*, between the outer and inner banks, rate of boundary dissolution or melting (for incised channels), or sediment discharge (for alluvial channels) to the strength of the secondary flow. In this step, the details of the erosion–deposition process are overlooked, and instead the lateral migration of the centroid of the incremental control volume is treated. Introduction of the secondary-flow equations into the closure relation yields a linear differential equation that is solved for its orthogonal components, which give the rates of meander growth and downstream migration. The expected meander wavelength is calculated as that with the fastest initial growth rate. The resulting analytical model is found to be applicable to all three types of channels, and to yield generally satisfactory predictions of the principal features of their meandering. Results reported by others are used in the verification of the analysis.

2. Analytical model

The flow to be analysed is depicted in figure 1, which also defines some of the notation. The channel cross-section may be treated as rectangular, because the analysis is concerned with the initial stages of meander development before the channel shape becomes distorted. Moreover, because an integral-type analysis is

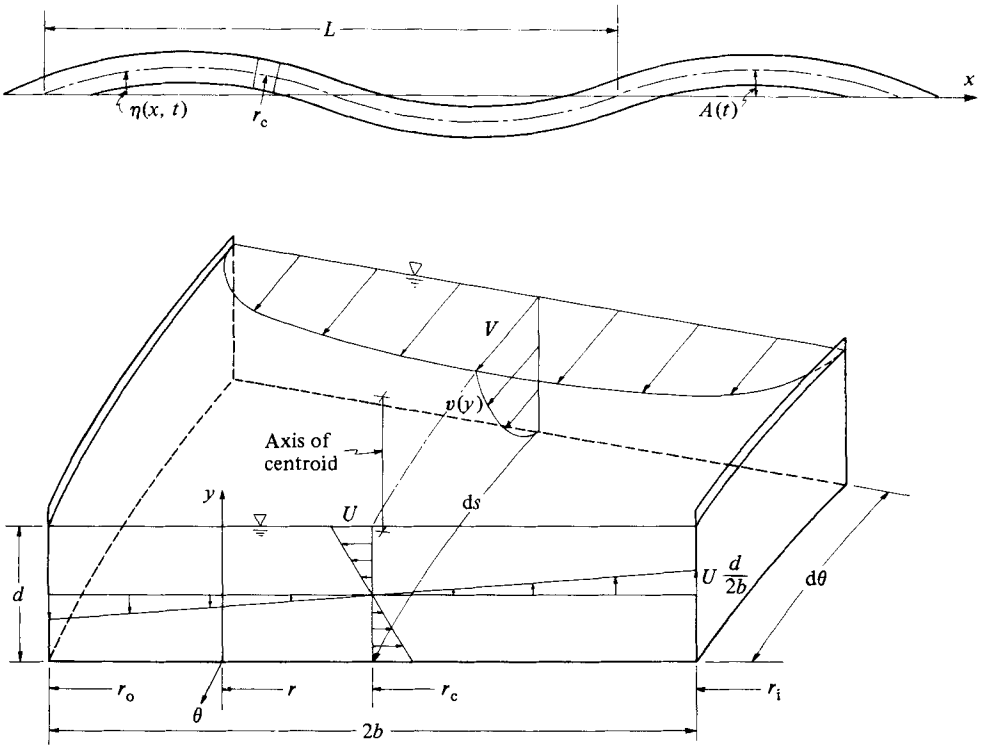

FIGURE 1. Definition sketch for sinusoidal-channel flow.

utilized, the details of the channel section, velocity distributions, etc are not critical. The primary flow is assumed to be uniform and quasi-steady. The latter assumption is justified on the grounds that the characteristic times associated with meander growth and migration are much smaller than the characteristic time of the primary flow.

The primary-flow velocity profile will be described by the power law

$$v = \begin{cases} V\left(\frac{y}{d}\right)^{1/n}\left(\frac{r_c+b-r}{b}\right)^{1/n} = \left(\frac{n+1}{n}\right)^2 \bar{V}\left(\frac{y}{d}\right)^{1/n}\left(\frac{r_c+b-r}{b}\right)^{1/n} & (r \geqslant r_c), \quad (1a) \\ V\left(\frac{y}{d}\right)^{1/n}\left(\frac{r-r_c+b}{b}\right)^{1/n} = \left(\frac{n+1}{n}\right)^2 \bar{V}\left(\frac{y}{d}\right)^{1/n}\left(\frac{r-r_c+b}{b}\right)^{1/n} & (r \leqslant r_c), \quad (1b) \end{cases}$$

where, in addition to the quantities defined in figure 1, $V \equiv$ surface velocity of primary flow at $r = r_c$, $r_c \equiv$ local radius of curvature of channel centreline, $\bar{V} \equiv$ mean (section-averaged) flow velocity, and $1/n \equiv$ velocity power-law exponent.

For calculation of the moment-of-momentum fluxes, it will be assumed that the vertical and horizontal components of the secondary current are linearly distributed, as depicted in figure 1. The strength of the former in relation to the latter shown in figure 1 is suggested by simple application of continuity to each channel-section quadrant. It is realized that these distributions violate the continuity equation locally, and also the boundary conditions. However, it was found that utilization of reasonable assumed distributions that do satisfy these requirements has only a minor effect on the computed moment-of-momentum flux and boundary shear stress.

Because these velocities are integrated over the cross-section, the details of their distributions are not particularly important. The strength of the secondary current will be calculated through application of the equation of conservation of moment of momentum. A detailed development of the analytical basis for this line of inquiry is presented by Jonsson (1982). It has been utilized previously in the analysis of flow in curved channels by Zimmermann & Kennedy (1978) and Falcón Ascanio & Kennedy (1983). In this type of formulation, the centrifugal torque about the flow's cross-section centroid (due to the interaction of channel curvature and the cross-sectional variability of primary-flow velocity) is set equal to the torque exerted by circumferential boundary shear stress and the streamwise rate of variation of the flux of moment-of-momentum, also computed about the cross-section centroid.

For a channel increment of length $\mathrm{d}s = r_c\,\mathrm{d}\theta$, the centrifugally induced torque about the centroid of the flow section is

$$\mathrm{d}T_c = \rho\overline{V}^2\left(\frac{n+1}{n}\right)^4\left\{\int_0^d\left(\frac{y}{d}\right)^{2/n}(y-\tfrac{1}{2}d)\,\mathrm{d}y \times\left[\int_{r_c-b}^{r_c}\frac{1}{r}\left(\frac{r-r_c+b}{b}\right)^{2/n}r\,\mathrm{d}r+\int_{r_c}^{r_c+b}\frac{1}{r}\left(\frac{r_c+b-r}{b}\right)^{2/n}r\,\mathrm{d}r\right]\right\}\mathrm{d}\theta$$

$$= \rho\overline{V}^2d^2b\frac{(n+1)^3}{n^2(n+2)^2}\mathrm{d}\theta \equiv H(n)\rho\overline{V}^2d^2b\,\mathrm{d}\theta, \tag{2}$$

where

$$H = \frac{(n+1)^3}{n^2(n+2)^2}. \tag{3}$$

The torque per unit length of channel centreline is then given by

$$\frac{\mathrm{d}T_c}{\mathrm{d}s} = H\rho\overline{V}^2d^2\frac{b}{r_c}. \tag{4}$$

This torque is partially balanced by that produced by boundary shear stress, which when computed about the centroid of the flow section is

$$\mathrm{d}T_n = \left(\tau_{1h}2b\frac{d}{2}+\tau_{1v}2bd\right)\mathrm{d}s, \tag{5}$$

where $\tau_{1h} \equiv$ horizontal component of shear stress on the bed, and $\tau_{1v} \equiv$ vertical component of shear stress on the banks. Because $U \ll \overline{V}$, where $U \equiv$ characteristic secondary-flow velocity, it may be assumed that these shear stresses are related to the average primary-flow boundary shear stress τ_0 through

$$\tau_{1h} = \alpha\tau_0\frac{U}{\overline{V}} \tag{6}$$

and

$$\tau_{1v} = \alpha\tau_0\frac{d}{2b}\frac{U}{\overline{V}}, \tag{7}$$

where α is a dimensionless coefficient of order one. From (5)–(7) there results

$$\frac{\mathrm{d}T_n}{\mathrm{d}s} = \alpha\tau_0P\frac{d}{2}\frac{U}{\overline{V}}, \tag{8}$$

where $P \equiv$ wetted perimeter of the channel. The flux of moment-of-momentum (about the section centroid) is given by

$$M = \rho\int_{A_f}\int v(\boldsymbol{u}\times\boldsymbol{l})\,\mathrm{d}A_f, \tag{9}$$

where $\boldsymbol{u} \equiv$ velocity of the secondary current in the plane of the flow section, $\boldsymbol{l} \equiv$ distance from the centroid of the flow section, and $A_f \equiv$ area of flow section. Note that the primary-flow velocity is perpendicular to the flow section, and therefore terms involving its cross-product do not enter (9). After a somewhat lengthy computation (see Appendix), M is obtained as

$$M = G\rho bd^2 \overline{V} U, \tag{10}$$

where, for the assumed velocity distributions in a rectangular channel,

$$G = \frac{4n^2+n+1}{(2n+1)(3n+1)}. \tag{11}$$

The moment-of-momentum equation under quasi-steady flow conditions, for the control volume bounded by the channel boundaries, the free surface, and the two planes $\theta = \text{const.}$ separated by centreline distance $\mathrm{d}s$, is

$$\frac{\mathrm{d}T_c}{\mathrm{d}s} - \frac{\mathrm{d}T_n}{\mathrm{d}s} = \frac{\mathrm{d}M}{\mathrm{d}s}. \tag{12}$$

Substitution of (4), (8) and (10) into (12) yields

$$H\rho \overline{V}^2 d^2 \frac{b}{r_c} - \alpha\tau_0 P \frac{d}{2} \frac{U}{\overline{V}} = G\rho bd^2 \overline{V} \frac{\mathrm{d}U}{\mathrm{d}s}, \tag{13}$$

which can be simplified to

$$\frac{\mathrm{d}U}{\mathrm{d}s} + \frac{\alpha f}{8GR} U = \frac{H}{G} \frac{\overline{V}}{r_c}, \tag{14}$$

where $f = 8\tau_0/\rho\overline{V}^2$ is the Darcy–Weisbach friction factor, and $R = 2bd/P$ is the hydraulic radius.

The channel-alignment perturbation will be taken to be a migrating sinusoid

$$\eta(x,t) = A(t) \sin k(x-ct), \tag{15}$$

where $x \equiv$ coordinate distance along the unperturbed-channel axis (see figure 1), $k = 2\pi/L$ is the wavenumber, $L \equiv$ meander wavelength, $t \equiv$ time, and $c \equiv$ migration velocity of the meander pattern. The channel-centreline displacement $\eta(t)$ is limited to values much smaller than the meander wavelength (i.e. $kA \ll 1$). The centreline curvature is then

$$\frac{1}{r_c} \approx -\frac{\mathrm{d}^2\eta}{\mathrm{d}x^2} = k^2 A(t) \sin k(x-ct). \tag{16}$$

The differential equation for U is obtained by substituting (16) into (13):

$$\frac{\mathrm{d}U}{\mathrm{d}x} + \frac{\alpha f}{8GR} U = \frac{H\overline{V}k^2 A}{G} \sin k(x-ct). \tag{17}$$

The solution of this equation that is periodic and independent of the initial condition (i.e. the one valid for $x/R \gg 8G/\alpha f$) is

$$\frac{U}{\overline{V}} = \frac{8Hk^2RA}{[\alpha^2 f^2 + 64G^2R^2k^2]^{\frac{1}{2}}} \sin k\left(x - ct - \frac{\gamma}{k}\right), \tag{18}$$

where the phase shift γ, between U and the channel-axis displacement, is given by

$$\tan\gamma = \frac{8GR}{\alpha f} k \quad (0 < \gamma < \tfrac{1}{2}\pi). \tag{19}$$

If the inertial term is dominant over the friction term, then $\gamma \sim \frac{1}{2}\pi$, in which case the velocity of the secondary current attains its maxima near the channel-axis inflections. In the other limiting case, $\gamma \sim 0$, and the secondary current is nearly in phase with the channel displacement.

To continue the stability analysis, it is necessary to adopt a closure equation relating the local rate of lateral displacement of the channel to the *differential* (between concave and convex banks) melting or dissolution in the case of incised ice or rock channels, or to *differential* scour and deposition in meandering alluvial channels. Note that the channel may be degrading, aggrading, shifting laterally, or even growing or becoming smaller this time, without affecting the analysis, which is concerned only with the local cross-channel differences in transport rates (of sediment, dissolved material, or heat) which produce meandering. The local details of the geometry and kinematics of meander growth and downstream migration will not be considered; instead the overall lateral movement of the incremental control volume shown in figure 1 will be examined. As the control volume shown in figure 1 moves laterally, owing to differential erosion, melting, or dissolution, the difference between the rates of these processes at the concave and convex banks is given by

$$\mathrm{d}Q_{\mathrm{L}} = dv_{\mathrm{G}}\,\mathrm{d}s, \tag{20}$$

where $v_{\mathrm{G}} \equiv$ rate of local lateral displacement of the centroid of the elemental control volume of length $\mathrm{d}s$ utilized in the moment-of-momentum analysis. Because the channel centreline is curved, the centroid of the control volume is not at midwidth of the channel, but is displaced toward the concave bank, the displacement being inversely proportional to the radius of curvature. It can be easily shown that for a rectangular cross section, the displacement is $b/3r_{\mathrm{c}}$. Inclusion of this term in the calculation is critical; without it, no dominant wavelength is predicted by the model. The rate of lateral migration is then

$$v_{\mathrm{G}} = \frac{\partial}{\partial t}\left[\eta + \frac{b^2}{3r_{\mathrm{c}}}\right] \approx \frac{\partial}{\partial t}\left[\eta - \frac{b^2}{3}\frac{\partial^2\eta}{\partial x^2}\right]. \tag{21}$$

In meandering alluvial rivers the rate of differential erosion–deposition across the channel is proportional to the rate of a ficticious lateral transport of sediment from the outer to the inner bank. In supraglacial (or rock-incised) streams, the rate of differential melting is proportional to the difference between the rates of heat transfer (or rock dissolution or erosion) at the concave and convex banks. All of these transport processes are affected by the secondary current, and their rates increase with its strength. In the present analysis it will be assumed that the transfer rates are proportional to the velocity of the secondary current, or

$$\frac{\mathrm{d}Q_{\mathrm{L}}}{\mathrm{d}s} \sim U, \tag{22}$$

or, from (21) and (22),

$$\frac{\partial\eta}{\partial t} - \frac{b^2}{3}\frac{\partial^3\eta}{\partial t\,\partial x^2} = \lambda U, \tag{23}$$

where $\lambda \equiv$ positive dimensionless constant or proportionality. It turns out that the dominant wavelength and the corresponding phase shift are independent of λ. Stability analyses of this type usually introduce the perturbation velocity or shear stress into one or another transport relation, which is then linearized. The result is

a relation similar to (22) and (23). Substitution of (15) and (18) into (23) leads, after some algebraic manipulation, to

$$\frac{1}{A}\frac{\mathrm{d}A}{\mathrm{d}t} = kc\cot k(x-ct) + \frac{8\lambda\bar{V}RHk^2}{(1+\frac{1}{3}b^2k^2)\,[\alpha^2f^2+64k^2G^2R^2]^{\frac{1}{2}}}[\cos\gamma - \sin\gamma\cot k(x-ct)], \tag{24}$$

where γ is given by (19). Integration of (24) yields

$$\ln A(t) = \text{constant} - \left[1 - \frac{8\lambda\bar{V}RHk\sin\gamma}{[\alpha^2f^2+64k^2G^2R^2]^{\frac{1}{2}}}\frac{1}{c}\right]\ln|\sin k(x-ct)| + \frac{8\lambda\bar{V}RHk^2\cos\gamma}{(1+\frac{1}{3}b^2k^2)\,[\alpha^2f^2+64k^2G^2R^2]^{\frac{1}{2}}}t. \tag{25}$$

This relation can be satisfied only if

$$c = \frac{8\lambda\bar{V}RHk\sin\gamma}{[\alpha^2f^2+64k^2G^2R^2]^{\frac{1}{2}}}. \tag{26}$$

Then

$$A(t) = A_0\exp\left[\frac{\lambda\bar{V}H\alpha f}{8RG^2}\frac{\sin^2\gamma}{1+(\alpha^2f^2/192G^2R^2)\tan^2\gamma}t\right] = A_0\exp\left[\frac{\lambda\bar{V}H\alpha f}{8RG^2}\frac{\sin^2\gamma}{1+\beta^2\tan^2\gamma}t\right], \tag{27}$$

where $\beta^2 = \alpha^2f^2b^2/192G^2R^2$.

The exponent in (27) is positive for all k and for γ in the interval $0 < \gamma < \frac{1}{2}\pi$. Over this range of γ, the amplitude of the sinusoidal perturbation increases exponentially with time. The exponent is zero for $k = 0$ ($\gamma = 0$) and tends to zero again for $k \to \infty$ $\gamma = \frac{1}{2}\pi$). Consequently, there is a dominant wavenumber for which the rate of growth is maximum. This wavenumber is determined by substituting (27) into $\partial^2A/\partial t\,\partial k = 0$, which leads to

$$\tan\gamma = \beta^{-\frac{1}{2}}, \tag{28}$$

and yields for the dominant wavenumber

$$k = \left(\frac{\sqrt{3}}{8}\frac{\alpha f}{G}\frac{1}{Rb}\right)^{\frac{1}{2}}, \tag{29}$$

for which the phase shift obtained from (19) is

$$\gamma = \tan^{-1}\left(8\sqrt{3}\frac{G}{\alpha}\frac{1}{f}\frac{R}{b}\right)^{\frac{1}{2}} \quad (0 \leqslant \gamma \leqslant \tfrac{1}{2}\pi). \tag{30}$$

The corresponding celerity is

$$c = \lambda\bar{V}\frac{H}{G}\sin^2\gamma = \frac{8\sqrt{3}\,\lambda\bar{V}HR/b}{\alpha f + 8\sqrt{3}\,GR/b}. \tag{31}$$

Finally, the amplitude of the dominant wave is given by

$$A(t) = A_0\exp\left[\sqrt{3}\,\lambda\frac{H}{G}\sin^2\gamma\cos^2\gamma\frac{\bar{V}t}{b}\right] = A_0\exp\left[\frac{24\lambda H\bar{V}Rt}{\alpha f\left(1+\frac{8\sqrt{3}\,G}{\alpha f}\frac{R}{b}\right)^2b^2}\right]. \tag{32}$$

3. Discussion of results and comparison with data

The foregoing analysis demonstrates that secondary currents produced by small, spatially periodic perturbations in the alignment of an otherwise straight channel can cause the amplitude of the perturbations to increase with time, and produce downstream migration of the resulting meanders. The stability analysis is linear, and, strictly speaking, is therefore applicable only to small-amplitude meanders. However, the results of such analyses, and especially the expressions for the dominant frequency or wavelength, are often applied, with considerable success, to large-amplitude waves.

The dominant wavelength given by (29) is

$$L = \frac{2\pi}{k} = 2\pi\left(\frac{8G}{\sqrt{3}\,\alpha f} Rb\right)^{\frac{1}{2}}. \tag{33}$$

The predicted meander wavelength is seen to be proportional to the square roots of the hydraulic radius and the channel width, and inversely proportional to the square root of the friction factor. The coefficient G given by (11), is a monotonically increasing function of n. The exponent n is related to the friction factor by (Karim & Kennedy 1981)

$$n \approx f^{-\frac{1}{2}}. \tag{34}$$

Note that for the assumed geometry and velocity distributions G varies very slowly with n. For example, as f increases from 0.01 to 0.20, which corresponds to n decreasing from 10 to 2.2, G varies only from 0.63 to 0.55.

The foregoing results are not very sensitive to the assumed shape of flow section or to the distributions of the primary- or secondary-flow velocities. For example, for $f = 0.04$, which corresponds to $n = 5$, the wavelength relationship for a rectangular channel is

$$L = 10.4\left(\frac{Rb}{\alpha f}\right)^{\frac{1}{2}}. \tag{35}$$

The foregoing analysis was repeated for a semicircular channel, of radius b, flowing full. The primary flow velocity was radially distributed according to the power law, and the secondary-flow velocity was linearly distributed (corresponding to rigid-body) along every radius. The dominant wavelength, again for $n = 5$, was found to be

$$L = 8.4\left(\frac{Rb}{\alpha f}\right)^{\frac{1}{2}}, \tag{36}$$

which, except for a small change in the coefficient, is identical with (35).

The predicted phase shifts between the channel-axis waves and the secondary-flow strength for typical values of the independent variables is well above $\frac{1}{4}\pi$, indicating that the frictional torque is generally smaller than the torsional inertia. Such large phase shifts, which are associated with a strong tendency of the meanders to migrate downstream, have been observed in the case of weakly meandering channels (Gottlieb 1976; Falcón Ascanio 1979). Experiments conducted by the authors in weakly meandering ice-incised channels also suggest that meanders migrate much faster than they grow. However, data on flows on strongly curved channels indicate small phase shifts (Zimmermann 1974; Zimmermann & Kennedy 1978; Odgaard & Kennedy 1982) and pronounced rates of meander growth compared with migration velocities (Dahlin 1974). While it is realized that the linearized analysis may not be adequate

to describe the flow in strongly meandering channels, it is noteworthy that Dahlin's (1974) observation is consistent with the analytical model, (31) and (32), developed here, which indicates that the ratio of the rate of meander growth to migration velocity is

$$\frac{1}{c}\frac{\mathrm{d}A}{\mathrm{d}t} = \sqrt{3}\cos^2\gamma\frac{A(t)}{b} = \frac{\sqrt{3}\,A(t)/b}{1+\dfrac{8\sqrt{3}}{f}\dfrac{G}{\alpha}\dfrac{R}{b}}. \tag{37}$$

The ratio is seen to increase as the meander grows in amplitude. The theoretical analysis, (30) and (37), also indicates that for small depth-to-width ratios and for large friction factors, the meanders will exhibit a stronger tendency to grow than to migrate. The former result is in general agreement with available observations. Vincent's (1967) and Chang, Simons & Woolhiser's (1971) experiments have demonstrated that for large depth-to-width ratios meandering does not develop in laboratory flumes. Parker (1976) concluded from an examination of field and laboratory data that alluvial channels tend to remain straight when the depth-to-width ratio is larger than 0.1. The evidence on the effects of friction on meandering is less conclusive. Nevertheless, Tanner (1960) found from his experiments that it was necessary to introduce some roughness to the bed surface before his streams would meander. Quraishi (1944) observed that the development of meandering in initially straight channels in a sand-bed flume was always preceded by an increase in the friction through the formation of ripples.

The meander migration velocity, given by (31), is proportional to the mean-flow velocity and decreases with increasing friction factor. In the case of deep channels with small friction factor, the meander-migration velocity is independent of the depth-to-width ratio and the friction factor:

$$c = \lambda\frac{H}{G}\overline{V}. \tag{38a}$$

In the other limiting case, that of shallow rough channels, c is proportional to the depth-to-width ratio and inversely proportional to the friction factor:

$$c = 8\sqrt{3}\,\lambda\frac{H}{\alpha}\overline{V}\frac{R}{b}\frac{1}{f}. \tag{38b}$$

Figure 2 presents 158 sets of laboratory and 73 sets of field alluvial-stream data (summarized by Ikeda *et al.* 1981, p. 372), as well as 8 supraglacial meandering streams (Leopold & Wolman 1960; Dahlin 1974) plotted in the format of (33). It is seen that the conformity of the data to the relation is surprisingly good, over a remarkably broad range of channel size. Moreover, there appears to be no distinction in the plot between ice- and alluvial-channel meanders. The relation for the straight line through the points is

$$L = 20\left(\frac{Rb}{f}\right)^{\frac{1}{2}}, \tag{39}$$

which, for $G = 0.6$, a representative value, correspond to $\alpha = 0.27$, a reasonable value.

It is also of interest to compare the predicted meander wavelength, (33) or (39), with the corresponding expression obtained from other stability analyses. Anderson's

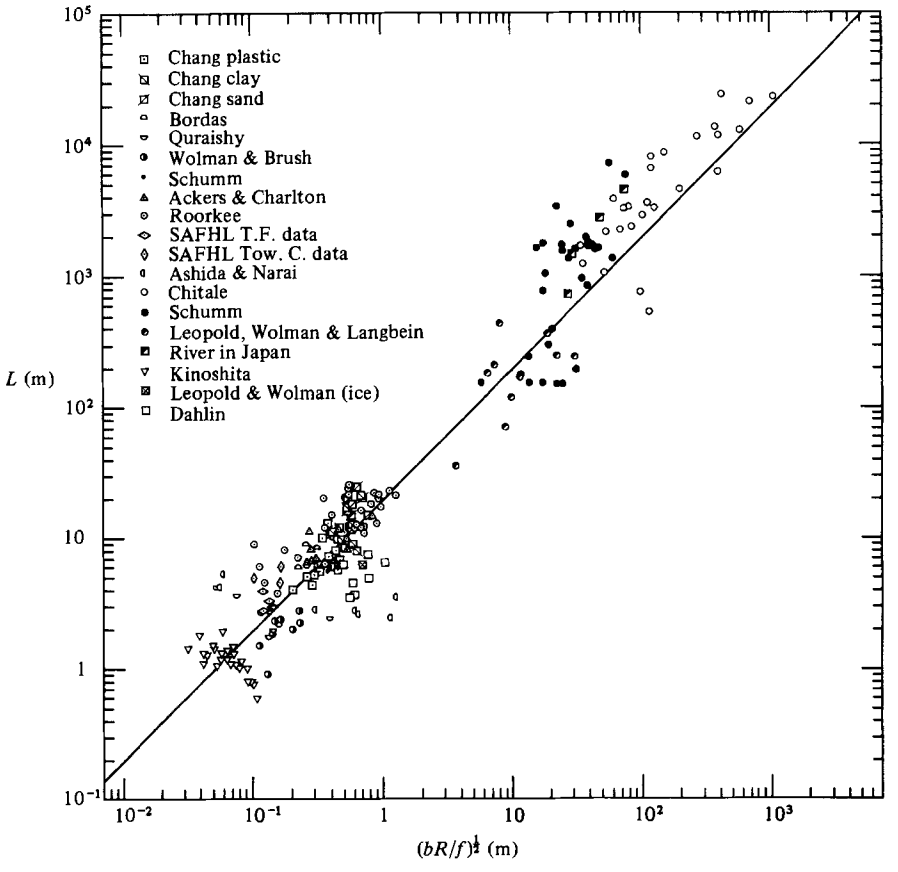

FIGURE 2. Alluvial and ice-incised channel data plotted in the form of (33).

(1967) theory based on the natural frequency of stationary transverse water waves yielded

$$L = 102(bd)^{\frac{1}{2}} F^{\frac{1}{2}}, \tag{40}$$

where $F \equiv$ Froude number. The constant, 102, was evaluated experimentally from flume data. The alluvial alternate-bar theory (Parker 1976) led to the expression

$$L = 8\pi^{\frac{1}{2}} \psi(F)\, F^{\frac{1}{2}} \left(\frac{bd}{f}\right)^{\frac{1}{2}}, \tag{41}$$

where $\psi(F) \equiv$ a function of the Froude number. For small values of the Froude number $\psi(F) \sim F^{-\frac{1}{2}}$, for which

$$L \sim \left(\frac{bd}{f}\right)^{\frac{1}{2}}. \tag{42}$$

It is noteworthy that the alluvial alternate-bar theory (Parker 1976), which utilizes the St Venant equations with depth-averaged quantities, and the theory developed here, which examines the secondary flow attendant to channel curvature, arrive at practically the same expression for the dominant meander length. However, the theory developed here is not necessarily limited to low-Froude-number flows.

Engelund & Hansen (1967) concluded that the meander length of alluvial streams

is determined mainly by the friction factor and the depth. Hansen's (1967) stability analysis suggested that in wide channels

$$L = 56\frac{d}{f}. \tag{43}$$

The bend stability theory of Ikeda *et al.* (1981) also emphasized the importance of depth and friction factor. For low-Froude-number flow in streams with an average transverse slope (based on field data) it yielded

$$L = 33.5\frac{d}{f}, \tag{44}$$

while for streams with laterally flat beds at low Froude numbers it gives

$$L = 16\pi F^{-1}\frac{d}{f}. \tag{45}$$

These theories give in most cases results of the same order of magnitude, so that it is not immediately obvious from comparison with data which mechanism is truly responsible for the initiation and development of meanders in streams. Unfortunately, most of the earlier experimental and data-collection efforts were mainly concerned with the derivation of relations between the meander wavelength or amplitude and the river discharge or stream width. Thus reliable measurements of friction factors and flow depths are seldom included in published data on stream meanders, particularly in the case of natural rock- and ice-incised streams. Furthermore, much of the scatter observed in comparisons between theoretical relations and data (such as figure 2) is due to sampling variability (related to the fact that the observed meander or bar lengths are seldom constant – Chang *et al.* 1971) and the selection of a dominant discharge (required to calculate depth, width and friction factor). Nevertheless, the dominant wavelength predicted by (39) was found to provide a somewhat better fit to the data used in figure 2 than the relations yielded by theories based on other physical considerations – (40) and (42)–(44).

4. Concluding remarks

An analytical model was developed to investigate the role of secondary flow in the initiation and early development of river meandering. The model shows that the amplitude of a small sinusoidal perturbation in the alignment of an initially straight channel tends to increase exponentially with time. The dominant wavelength and the corresponding phase shift between the channel-meander wave and the strength of the spiral motion were calculated. Analytical expressions were also developed for the rate of amplitude increase and the celerity of meander migration. The model developed here is limited to quasi-steady flow in weakly meandering prismatic channels.

The results of the analytical model are in good agreement with data on meandering streams. The expression developed for the phase shift between the local secondary-flow strength and the local channel curvature is in conformity with values observed in weakly meandering sinuous channels. The expression for the dominant wavelength, even though developed from a small-perturbation analysis, is in surprisingly good agreement with measured wavelengths of meandering alluvial, rock-incised and ice-incised streams.

The secondary-current instability theory developed herein and the alluvial alternate-bar instability theory of Parker (1976) arrive at practically the same relationship for the dominant wavelength. Furthermore, the meander wavelength predicted by the bend theory (Ikeda *et al.* 1981) and the present secondary-current theory are of the same order of magnitude. It is therefore not possible at this point to conclude through validation of existing theories with available data which mechanism (or mechanisms) is responsible for the initiation and development of meanders. Three-dimensional stability analyses examining all mechanisms of meander initiation would be useful in resolving this issue, but would likely be difficult to develop. Cleverly designed experiments in which the competing mechanisms are controlled are likely to be required before the question is resolved.

This paper is based on work supported by the National Science Foundation under Grant CEE 81-09252. The authors are indebted to Professor Gary Parker for his assistance in providing data and copies of figures prepared by him.

Appendix

The moment-of-momentum flux corresponding to the vertical component of the secondary-current velocity is

$$\begin{aligned} M_{\mathrm{v}} &= 2\rho \int_0^b \mathrm{d}l \int_0^d \mathrm{d}y\, U \frac{d}{2b}\left(1-\frac{l}{b}\right)(b-l)\left(\frac{n+1}{n}\right)^2 \bar{V}\left(\frac{y}{d}\right)^{1/n}\left(\frac{l}{b}\right)^{1/n} \\ &= \left(\frac{n+1}{n}\right)^2 \rho b d^2 U \bar{V} \int_0^b \left(1-\frac{l}{b}\right)^2 \left(\frac{l}{b}\right)^{1/n} \frac{\mathrm{d}l}{b} \int_0^h \left(\frac{y}{d}\right)^{1/n} \frac{\mathrm{d}y}{d} \\ &= \left(\frac{n+1}{n}\right)^2 \rho b d^2 U \bar{V} \frac{2n^3}{(n+1)(2n+1)(3n+1)} \frac{n}{n+1} \\ &= \frac{2n^2}{(2n+1)(3n+1)} \rho b d^2 U \bar{V}, \end{aligned}$$

where in this Appendix $l \equiv$ distance from the bank closest to the point. The factor $d/2b$ is suggested by continuity considerations of the secondary flow.

The moment-of-momentum flux corresponding to the horizontal component of the secondary-current velocity is

$$\begin{aligned} M_{\mathrm{h}} &= 2\rho \int_0^b \mathrm{d}l \int_0^d \mathrm{d}y\, \bar{V}\left(\frac{n+1}{n}\right)^2 \left(\frac{l}{b}\right)^{1/n}\left(\frac{y}{d}\right)^{1/n}\left(1-2\frac{y}{d}\right) U(\tfrac{1}{2}d-y) \\ &= \rho U \bar{V}\left(\frac{n+1}{n}\right)^2 b d^2 \int_0^b \left(\frac{l}{b}\right)^{1/n} \frac{\mathrm{d}l}{b} \int_0^h \left(\frac{y}{d}\right)^{1/n}\left(1-\frac{2y}{d}\right)^2 \frac{\mathrm{d}y}{d} \\ &= \rho U \bar{V}\left(\frac{n+1}{n}\right)^2 b d^2 \frac{n}{n+1} \frac{n(2n^2+n+1)}{(n+1)(2n+1)(3n+1)} = \frac{2n^2+n+1}{(2n+1)(3n+1)} \rho b d^2 U \bar{V}. \end{aligned}$$

Consequently

$$M = M_{\mathrm{v}} + M_{\mathrm{h}} = \frac{4n^2+n+1}{(2n+1)(3n+1)} \rho b d^2 U \bar{V}.$$

REFERENCES

ANDERSON, A. G. 1967 On the development of stream meanders. In *Proc. 12th Congr. IAHR, Fort Collins, Colorado*. Vol. 1, pp. 370–378.

ASHIDA, K. & SAWAI, K. 1977 A study on the stream formation process on a bare slope. 3. *Ann. Disaster Prevention Res. Inst.* 20B-2, *Kyoto University*.

CALLANDER, R. A. 1968 Instability and river meanders, Ph.D. thesis University of Auckland.

CALLANDER, R. A. 1978 River meandering. *Ann. Rev. Fluid Mech.* **10**, 129–158.

CHANG, H., SIMONS, D. B. & WOOLHISER, D. A. 1971 Flume experiments on alternate bar formation. *J. Waterways, Harbors, Coastal Engng Div. ASCE* **97**(WWI), 155–165.

DAHLIN, B. 1974 A contribution to the study of meandering. M.Mc. thesis, Dept of Geology, Univ. Minnesota, Minneapolis.

ENGELUND, F. & HANSEN, E. 1967 *A Monograph on Sediment Transport in Alluvial Streams*. Danish Technical Press.

ENGELUND, F. & SKOVGAARD, O. 1973 On the origin of meandering and braiding in alluvial streams. *J. Fluid Mech.* **57**, 289–302.

FALCÓN ASCANIO, M. A. 1979 Analysis of flow in alluvial channel bends. Ph.D. thesis University of Iowa, Iowa City.

FALCÓN ASCANIO, M. A. & KENNEDY, J. F. 1983 Flow in alluvial-river curves. *J. Fluid Mech.* **133**, 1–16.

GOTTLIEB, L. 1976 Three-dimensional flow pattern and bed topography in meandering channels. *Series Paper* 11, *Inst. Hydrodyn. Hydraul. Engng Tech. Univ. Denmark, Lyngby*.

HANSEN, E. 1967 The formation of meanders as a stability problem. *Basic Res. Prog. Rep.* 13, *Hydraul. Lab., Tech. Univ. Denmark, Lyngby*.

HAYASHI, T. 1973 On the cause of meandering of rivers. *Proc. IAHR Symp. on River Mech., Paper* A-57, *Bangkok*.

IKEDA, S., PARKER, G. & SAWAI, K. 1981 Bend theory of river meanders. Part 1. Linear development. *J. Fluid Mech.* **112**, 363–377.

JONSSON, I. G. 1982 The angular momentum equation and its application to water waves, part 1: theory. *Prog. Rep.* 56, pp. 35–45, *Inst. Hydrodyn. Hydraul. Engng Tech. Univ. Denmark, Lyngby*.

KARIM, F. & KENNEDY, J. F. 1981 Computer-based predictors for sediment discharges and friction factors of alluvial streams. *IIHR Rep.* 242, *Iowa Inst. Hydraul. Res., Univ. Iowa, Iowa City*.

KELVIN, LORD 1876 On the winding of rivers in alluvial plains. *Proc. R. Soc. Lond.* A **25**, 5–8.

LELIAVSKY, S. 1955 *An Introduction to Fluvial Hydraulics*. Constable.

LEOPOLD, L. B. & WOLMAN, M. G. 1960 River meanders. *Bull. Geol. Soc. Am.* **71**, 769–794.

ODGAARD, A. J. & KENNEDY, J. F. 1982 Analysis of Sacramento River bend flows and development of a new method for bank protection. *IIHR Rep.* 241, *Iowa Inst. Hydraul. Res., Univ. Iowa, Iowa City*.

PARKER, G. 1975 Meandering of supraglacial melt streams. *Water Resources Res.* **11**, 551–552.

PARKER, G. 1976 On the cause and characteristic scales of meandering and braiding in rivers. *J. Fluid Mech.* **76**, 457–480.

PARKER, G. & ANDERSON, A. G. 1975 Modelling of meandering and braiding in rivers. In *Proc. ASCE Modelling Symp., San Francisco*, pp. 575–591.

PARKER, G., SAWAI, K. & IKEDA, S. 1982 Bend theory of river meanders. Part 2. Nonlinear deformation of finite-amplitude bends. *J. Fluid Mech.* **115**, 303–314.

QUARAISHI, M. S. 1944 The origin of curves in rivers. *Current Sci.* **13**, 36–39.

TANNER, W. F. 1960 Helicoidal flow, a possible cause of meandering. *J. Geophys. Res.* **65**, 993–995.

VINCENT, J. 1967 Effect of bedload movement on the roughness coefficient value. In *Proc. 12th Congr. IAHR, Fort Collins, Colorado*, vol. 1, pp. 162–171.

ZIMMERMANN, C. 1974 Sohlausbildung, Reibungfaktoren und Sedimenttransport in Gleichformig Gekrummten und Geraden Gerinnen. Ph.D. thesis, Institute Hydromechanics, University of Karlsruhe.

ZIMMERMANN, C. & KENNEDY, J. F. 1978 Transverse bed slopes in curved alluvial streams. *J. Hydraul. Div. ASCE* **104** (HY1), 33–48.